Plots were made of the logarithm of γ_R (activity coefficient of chlorofluoromethanes) vs. the reciprocal of absolute temperature at various compositions. The resulting curves were essentially straight lines in all cases, and the slopes were taken equal to the partial derivative. Figure 4 indicates the results found for $\Delta\bar{H}_R$ as a function of composition for the system of chlorodifluoromethane and tetraethylene glycol dimethyl ether.

In general ΔH_R can be expressed fairly well by a quadratic function such as

$$\Delta\bar{H}_R = A + B\,x_R + Cx_R^2 \qquad (11)$$

Since at $x_R = 1.0$ (pure R), $\Delta\bar{H}_R = 0$

$$\Delta\bar{H}_R = A(1 - x_R^2) + B(x_R - x_R^2) \qquad (12)$$

Substituting Equation (12) into Equation (9), integrating and noting that $\Delta H_T{}^M = 0$ at $n_R = 0$ one gets

$$\Delta H^M = \frac{\Delta H_T{}^M}{(n_R + n_S)} = -(2A + B)x_S \ln x_S - (A + B)x_R x_S \qquad (13)$$

The constants A and B were evaluated by the method of least squares to be -2.62 and 0.905 respectively for the system of chlorodifluoromethane and tetraethylene glycol dimethyl ether. Figure 4 indicates that the analytical expression gives a fair fit to the data. An expression for this system may be obtained by substituting A and B into Equation (13):

$$\Delta H^m = 4.33\,x_S \ln x_S + 1.71\,x_R x_S \qquad (14)$$

Figure 5 indicates the relatively good agreement between the calculated and the experimental values (9) at 3.5°C. Although several assumptions were made, the method seems reliable within about 10%. Improved agreement might be expected with a better equation than Equation (11) for fitting the $\Delta\bar{H}_R$ data. The accuracy of the present results probably does not justify such a refinement.

ACKNOWLEDGMENT

Indiana Gas Association sponsored this project through Purdue Research Foundation.

NOTATION

a_i = activity of component i at T and p of solution, $a_i = 1.0$ at $x_i = 1.0$
f = functionality of solvent, active sites per molecule
f_R° = fugacity of pure liquid R at T and p of solution
f°_{RG} = fugacity of pure gaseous R at T and p of solution
ΔH_R° = standard enthalpy of reaction, k.cal./g. mole of complex
$\Delta\bar{H}_R$ = partial molal enthalpy change of component R in mixture
$\Delta H_T{}^M$ = total enthalpy change of mixture on mixing at constant T and p, cal.
ΔH^m = heat of mixing at constant T and p, cal./g. mole of solution
n_i = moles of component i
p = pressure
p_{RG} = partial pressure of refrigerant vapor, lb./sq.in.abs.
p°_{RG} = vapor pressure of pure refrigerant, lb./sq.in.abs.
T = absolute temperature, °K.
x_i = liquid mole fraction of component i
γ_i = activity coefficient of component i, $\gamma_i = 1.0$ at $x_i = 1.0$

LITERATURE CITED

1. Albright, L. F., P. C. Buclez, C. R. Pluche, and T. C. Doody, *Am. Soc. Heating, Refrig., Air-Conditioning Engrs. Trans.*, **66**, 423 (1960).
2. Albright, L. F., and J. D. Lawyer, *Am. Soc. Heating, Refrig., Air-Conditioning Journal*, **1**, No. 4, p. 67 (1959).
3. Albright, L. F., and A. S. Mandelbaum, *Refrig. Eng.*, **64**, No. 10, p. 37 (1956).
4. E. I. duPont de Nemours and Co., Inc., bulletin, Thermodynamic Properties of Freon-21 (1939); Thermodynamic Properties of Freon-22 (1945); and Private communication from J. J. Martin, University of Michigan, Ann Arbor, Michigan (1960).
5. Mastrangelo, S. V. R., *J. Phys. Chem.*, **63**, 608 (1959).
6. ———, *Am. Soc. Heating, Refrig., Air-Conditioning Engrs. Journal*, **1**, No. 10, p. 64 (1960).
7. Terrier, Francois, M.S. thesis, Purdue Univ., Lafayette, Indiana (1961).
8. Thieme, A. A., and L. F. Albright, *Am. Soc. Heating, Refrig., Air-Conditioning Journal*, **3**, No. 7, p. 71 (1961).
9. Zellhoefer, G. F., and M. J. Marvel, *J. Am. Chem. Soc.*, **60**, 1343 (1938).

Manuscript received December 1, 1961; revision received March 5, 1962; paper accepted March 7, 1962. Paper presented at A.I.Ch.E. New Orleans meeting.

Drop Formation from Rapidly Moving Liquid Sheets

R. P. FRASER, PAUL EISENKLAM, NORMAN DOMBROWSKI, and DAVID HASSON

Imperial College, London, England

In a widespread range of spraying applications atomization is achieved by a nozzle which transforms the liquid into an unstable sheet.

A former investigation of spray sheets in atmosphere (*1*) has established two principal modes of disintegration. Within a limited range of conditions sheets may remain undisturbed and disintegrate into a network of unstable ligaments produced by the coalescence of expanding perforations. A sheet is however normally disturbed by aerodynamic waves. Fragments of liquid are broken off the wavy sheet and, although suffering continuous disintegration by air action, tend to contract into unstable ligaments.

The ambient atmosphere is thus one of the significant factors contributing to the instability and disintegration of a liquid sheet. This investigation examines the separate effects of ambient atmosphere and liquid velocity on the mode of breakup of a sheet not rendered unstable by air action and determines the characteristic drop sizes resulting from sheets undergoing different modes of disintegration.

Flat spray sheets, produced by single-hole fan spray nozzles, have been selected for investigation because they are convenient for both analytical

David Hasson is presently with the Technicon, Haifa, Israel.

and experimental study while retaining the essential breakup features of other spray sheets.

The sheets have been studied visually by flash photography, while the resulting spray has been sampled by a collection technique. It has been found that the mode of disintegration is critically dependent upon the ambient density because the wavy sheet suddenly changes to a perforated sheet as a partial vacuum is attained. This effect is associated with a sudden increase in the drop size of the spray.

An additional form of instability produced by liquid turbulence has been isolated and examined in vacuum. The transition to turbulent flow has no marked effect on the drop size.

Previous analyses of the aerodynamic instability of liquid sheets of uniform thickness have been critically reviewed and satisfactorily applied to the flow of attenuating liquid sheets. The results have been extended to provide a theoretical basis for predicting the effects of several factors on the drop size. The predictions are compared with experimental data.

AERODYNAMICAL INSTABILITY OF A LIQUID SHEET

Consider the system of forces acting on the slightly disturbed interface of a liquid sheet moving in air (Figure 1). Surface tension force tends to draw the liquid back to its original position, while the air, acquiring an increased velocity and hence creating a local decrease in pressure in the vicinity of the protuberance, pulls the liquid outward. Under certain conditions aerodynamic forces exceed the interfacial tension and cause the formation of unstable waves which propagate at the same velocity as the sheet and with exponentially increasing amplitude.

The mathematical procedure to determine instability consists of assuming that a small periodic disturbance is imposed on the system and analyzing the amplitude growth rate which may be defined by

$$y = y_o e^{\beta t} \qquad (1)$$

If it is found that β is real and positive, the amplitude y increases exponentially, and the system is therefore unstable. Otherwise the system is stable.

Two types of oscillations have to be considered, namely antisymmetric (sinuous) and symmetric (dilational) modes (Figure 2). For the former the displacements of corresponding points are in the same direction (sinuous waves), and for the latter the displacements are in the opposite direction (dilational waves). A hypothetical liquid sheet having no free edges is stable under the action of surface tension forces alone (*10*), contrary to a jet for which under similar conditions symmetrical oscillations are unstable (varicose jet) (*11, 12*). In a jet either type of wave may predominate depending upon the conditions. However dilational waves in a sheet may be neglected since their degree of instability is always less than that of sinuous ones (*13, 14*). In the authors' experiments only sinuous waves were in fact observed.

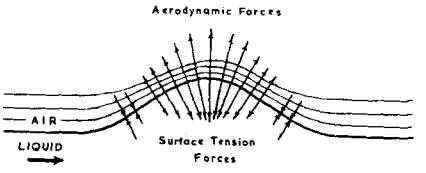

Fig. 1. Aerodynamic forces acting at interface.

In analyzing the more unstable antisymmetrical oscillations of a liquid sheet moving in still air Squire (*13*) has derived the following expression for the amplitude growth rate:

$$\frac{h'\beta}{U_o} = \frac{\left\{\frac{kh'}{N_{we}}\left[\rho(N_{we}-1) - kh'\right]\right\}^{1/2}}{1+\frac{\rho}{kh'}} \qquad (2)$$

An approximation included in Equation (2) is that $\tanh kh' \approx kh'$. This is valid for all practical purposes, since usually $kh' < 0.25$.

The minimum wave length for an unstable system is found from $\beta = 0$. Hence

$$kh' = \rho(N_{we}-1) \qquad (3)$$

or

$$\lambda_{min} = \frac{2\pi h'}{\rho(N_{we}-1)} \qquad (4)$$

and since usually $N_{we} >> 1$

$$\lambda_{min} = \frac{2\pi\gamma}{\rho_a U_o^2} \qquad (5)$$

Equation (2) also provides an instability criterion based on the flow conditions: for β to be real $N_{we} > 1$.

The optimum wave length is that which has a maximum growth rate. It is obtained from

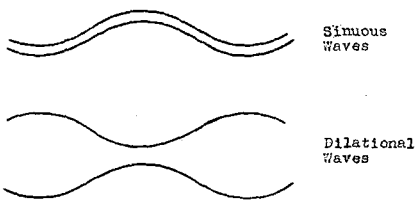

Fig. 2. Sinuous and dilational waves.

$$\frac{d\left[\frac{h'\beta}{U_o}\right]}{d(kh')} = 0 \qquad (6)$$

In differentiating Equation (2) the denominator may be regarded as unity since usually $\frac{\rho}{kh'} << 1$. A maximum for $\left(\frac{h'\beta}{U_o}\right)$ occurs at

$$kh' = \frac{\rho}{2}(N_{we}-1) \qquad (7)$$

so that

$$\lambda_{opt} = \frac{4\pi h'}{\rho(N_{we}-1)} \qquad (8)$$

and

$$\left[\frac{h'\beta}{U_o}\right]_{max} = \frac{\rho(N_{we}-1)^2}{2(N_{we})^{1/2}(N_{we}+1)} \qquad (9)$$

For $N_{we} >> 1$

$$\lambda_{opt} = \frac{4\pi\gamma}{\rho_a U_o^2} \qquad (10)$$

and

$$\left[\frac{h'\beta}{U_o}\right]_{max} = \frac{\rho(N_{we})^{1/2}}{2} \qquad (11)$$

Another significant equation in Squire's analysis is

$$\frac{w}{U_o k} = \frac{V}{U_o} = \frac{1}{1+\rho\coth kh'} \qquad (12)$$

Since $\rho\coth kh' << 1$, it follows that $V = U_o$; that is the waves travel at the same velocity as the sheet.

In a second analysis of the same problem Hagerty and Shea (*14*) obtained a very similar solution, the only difference being the prediction of instability, namely $N_{we} > 0$. This implies that provided the initial disturbance is able to supply all necessary frequencies, as may be assumed to occur in practice, instability should occur for all flow conditions. The relations for λ_{opt} and $\left[\frac{h'\beta}{U_o}\right]_{max}$ become identical to those of Squire for the practical range where $\tanh kh' \approx kh'$, $\frac{\rho}{kh'} << 1$, and $N_{we} >> 1$.

In testing theory with experiment Hagerty and Shea confirmed the amplitude growth rate equation from photographs of sheets with induced vibrations. Squire used photographs of swirl spray sheets at subatmospheric densities to verify the equation for the most unstable wave length [Equation (10)] but pointed out some uncertainty in the comparison, since accurate data for film thickness and velocity were not available.

ANALYSIS OF THE DROP SIZE FROM AN AERODYNAMICALLY UNSTABLE LIQUID SHEET

The main features of aerodynamic instability of sheets of uniform thick-

ness are adequately represented by the analyses discussed in the previous section. In this section an attempt will be made to extend these theories to provide a theoretical expression for the drop size of a low viscosity fan spray sheet. An analysis of the flow in a fan spray sheet, published elsewhere (9), shows that the streamlines diverge radially from the orifice and that the velocity along each streamline remains constant. The film thickness h at any point is found to be related to the radial distance r from the orifice by the simple relationship

$$hr = k_o \qquad (13)$$

The approach can be justified on the grounds that both Squire (13) and the authors (as will be discussed later in this paper) have found reasonable agreement between the value of the wave lengths of sinuous waves produced on attenuating sheets and those predicted for sheets of constant thickness. This probably results from the fact that in the region of disintegration of a sheet the rate of change of thickness is very small.

The following idealized breakup mechanism will be assumed. The most rapidly growing (β_{max}) wave is detached at the leading edge in the form of a ribbon half a wave length wide $\left(\frac{\lambda_{opt}}{2}\right)$. This ribbon immediately contracts into a ligament of radius r_l which subsequently disintegrates into drops of equal diameter. A diagrammatic representation of this mechanism is shown in Figure 3.

If one equates volumes of ribbon and ligament it is seen that

$$r_l = \left[\frac{\lambda_{opt}\, h^*}{2\pi}\right]^{1/2} \qquad (14)$$

In accordance with Rayleigh's analysis (11) the collapse of a ligament produces drops of diameter

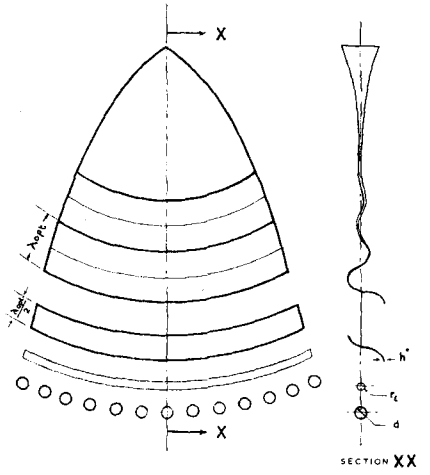

Fig. 3. Successive stages in the idealized breakup of a wavy sheet.

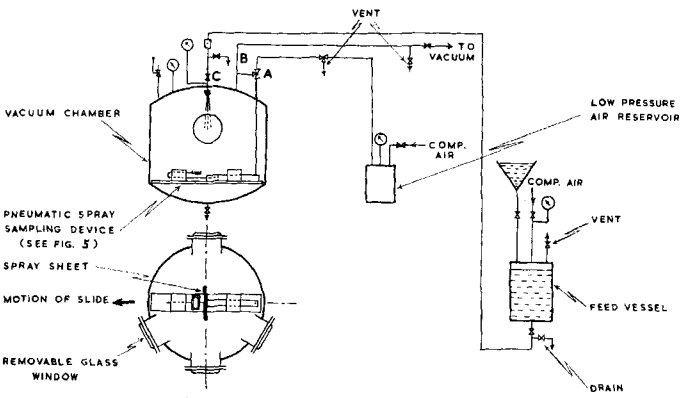

Fig. 4. Layout of vacuum chamber and apparatus for drop size experiments.

$$d = 3.78\ r_l \qquad (15)$$

and hence

$$d = \text{const}\ [\lambda_{opt}\, h^*]^{1/2} \qquad (16)$$

As shown by both Squire's and Hagerty and Shea's analyses the wave length of the most unstable wave and its corresponding growth rate are given by

$$\lambda_{opt} = \frac{4\pi\gamma}{\rho_a U_o^2} \qquad (10)$$

and

$$\frac{\beta_{max}\, h^*}{U_o} = \rho (N_{we})^{1/2} \qquad (11a)$$

Rearranging one obtains

$$\beta_{max} = \frac{U_o\, \rho (N_{we})^{1/2}}{h^*} \qquad (17)$$

where N_{we} is based on h^*.

The amplitude growth rate of the most unstable wave may be represented by Equation (1) transformed as follows:

$$\beta_{max} t = \ln \frac{y^*}{y_o} = E \qquad (18)$$

Substituting for β_{max} in Equation (18) one gets

$$U_o t \frac{\rho (N_{we})^{1/2}}{h^*} = E \qquad (19)$$

Now $U_o t$ is the breakup length r^*, and $r^* = \frac{k_o}{h^*}$ [Equation (13)], so that

$$\frac{\rho\, k_o\, (N_{we})^{1/2}}{(h^*)^2} = E \qquad (20)$$

Rearranging one sees that the film thickness at breakup is given by

$$h^* = \left[\frac{1}{2E^2}\right]^{1/3} \left[k^2 \frac{\rho_a^2 U_o^2}{L\gamma}\right]^{1/3} \qquad (21)$$

The only unknown term is $E = \ln \frac{y^*}{y_o}$, the ratio of the amplitude at breakup to the initial one at the orifice. In the investigation of jets disintegrating by rotationally symmetrical oscillations (12) it has been established that the condition for breakup is that the ratio y^*/y_o reaches a universally constant value. It will be assumed that a similar criterion applies to the disintegration of a liquid sheet.

This assumption has been tested for the fan spray sheet with measured values of h^* obtained at varying air density and liquid velocity. It has been confirmed that for a given nozzle the ratio E [calculated from Equation (20)] remains in fact constant. However there appears to be a tendency for a slow decrease of E with increasing k_o. This will be neglected as there are insufficient data to establish a more accurate breakup criterion.

The final expression giving the mean drop diameter is obtained by combining Equations (10), (16), and (21):

$$d = \text{const} \left[\frac{\rho_L}{\rho_a}\right]^{1/6} \left(\frac{k_o \gamma}{\rho_L U_o^2}\right)^{1/3} \qquad (22)$$

Now $\Delta p = \frac{\rho_L U_o^2}{2 g_c C_v^2}$

For fan spray nozzles $C_Q \approx C_v$ (9) and lies between 0.8 and 0.95. Thus

$$d = \text{const} \left[\frac{k_o \gamma}{C_Q^2 \Delta p}\right]^{1/3} \left[\frac{\rho_L}{\rho_a}\right]^{1/6} \qquad (23)$$

All previously derived formulas for the mean drop size of any type of spray sheet, flat or conical, are essentially similar to this equation; the latter is however more general because it includes the air density hitherto not considered. For example in a rigorous mathematical treatment of the breakup of a flat sheet of uniform thickness

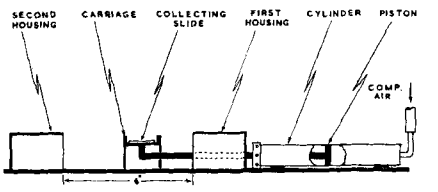

Fig. 5. Schematic diagram of pneumatic spray sampling device.

Keller and Kolodner (29) have shown that

$$d = \text{const}\left(\frac{\gamma h^2}{\Delta p}\right)^{1/3}$$

while Dorman (27) using dimensional analysis found a similar expression to Equation (23) except for the missing air density term.

APPARATUS AND EXPERIMENTAL METHODS

The layout of the equipment is shown in Figure 4. Water was injected through a nozzle into a vacuum chamber by applying compressed air to a feed vessel. No attempt was made to isolate the compressed air from the water, since experiments had shown that dissolved gases have no effect on the disintegration of a spray sheet.

The design of the cylindrical chamber used for drop size measurement and the photographic study of sprays can be seen from Figure 4. The chamber was of 2½ cu. ft. capacity, 18 in. internal diameter, and 20 in. overall height. Four removable glass portholes were incorporated around the cylindrical body to allow photography and access to the inside of the chamber. The spray nozzle was screwed to an adjustable feed pipe which was held vertically in the center of the chamber cover plate.

Drops were captured on a cavity slide filled with oil which was moved across the spray by a pneumatic device supported at the bottom of the vacuum chamber. Its construction is illustrated in Figure 5. The carriage holding the sampling slide was attached to a piston moving inside a cylinder. The piston, driven by low pressure air, pulled the carriage across the spray from a first to a second housing.

A minority of coarse drops are unavoidably formed at the rims of the fan spray sheet. Hence to obtain a sample of drops representative of the main spray only the collecting slide was moved along a line normal to the plane of the spray and intersecting the vertical axis (see Figure 4). During sampling the slide traveled a total distance of 6 in., symmetrical about the vertical axis at a depth of 15 in. from the nozzle tip.

The composition of the oil chosen for collecting samples of water sprays was as recommended in Reference 2.

To prevent the oil on a slide from frothing in vacuum and hence creating bubbles which are indistinguishable from drops, volatile components of the oil were distilled off in a vacuum oven held at a temperature between 30° and 40°C.

All experiments were carried out over a free water surface at a temperature of approximately 60°F. Thus even under low ambient pressures variation in drop size caused by evaporation could be ignored.

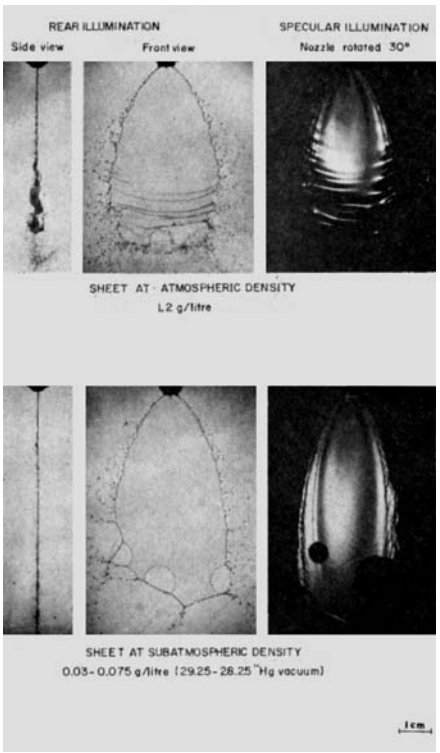

Fig. 6. Liquid sheet at atmospheric and at subatmospheric density.

Counting and Analysis of Drops in a Sample

A portion of the drops collected in an experiment was recorded on a photomicrograph at a magnification of x8. The fine drops, missing from the slide by nonimpingement, were neglected. The drop size distribution was measured from the photographic negative, projected on a screen to give an exact total magnification of x100. The size intervals chosen in grouping the drop diameters were such that the volumes of drops from successive classes were in a geometrical progression. The number of drops counted from each sample was between 1,000 and 3,000.

It may be noted that there is no clear indication of the number to be used in order to secure an accurate estimate of the true drop size. Such meager information as is available (3, 4, 5) indicates that for the above number of drops that were conveniently counted and sized the error may be of the order of ± 10%. For this reason an independent repeat of each drop size experiment was carried out.

The mean chosen to represent the drop size distributions was the surface-volume (or Sauter) mean diameter. In calculating this mean diameter the integration method suggested by Heywood (6) was used rather than a simplified procedure based on any fitted mathematical distribution, since statistical tests (2, 3), show the former method to give the most accurate estimate of this surface mean diameter.

It is difficult to derive a rational expression for the size dispersion, and there is no generally accepted definition of this parameter. The one used here is defined as a fractional drop size range based on the surface-volume mean diameter:

$$q = \frac{d_{5\%} - d_{95\%}}{d_s}$$

Fan Spray Nozzles

Single hole fan spray nozzles were used (9). Table 1 gives the dimensions of the rectangular orifices and the flow characteristics of the nozzles.

The flow number is given by

$$FN = \frac{Q}{\sqrt{\Delta p}} = \frac{294\, C_Q \cdot A}{\sqrt{\rho_L}} \qquad (24)$$

where Q is in imperial gal./hr., Δp in lb./sq.in., A in sq. cm., and ρ_L in g./cc.

THE EFFECT OF SUBATMOSPHERIC AMBIENT DENSITIES ON DROP SIZE RESULTS AND MODE OF BREAKUP

To determine the effect of subatmospheric ambient density on disintegration two series of drop size experiments were carried out with distilled water. The same nozzle, namely $W(i)$ (Table 1), was employed throughout. In the first series of experiments the differential liquid pressure was held constant at 25 lb./sq.in., and air density was varied from atmospheric pressure to a vacuum of 28.75 in. Hg (corresponding to moist air densities of ρ_a = 1.21 to 0.050 g./liter). Figure 6 illustrates the wavy and perforated sheets obtained at the extreme air density levels, each sheet photographed from three directions.

Similar photographs* taken at intervals of 5.25 in. Hg show that the vigorous waviness persists down to an air density of 0.74 g./liter (11.5 in. Hg vacuum), the sheet becoming unruffled and perforated below an air density of 0.51 g./liter (17.25 in. Hg vacuum).

In the authors' experiments only sinuous waves have been observed and measurements of their wave lengths made from the photographs have been used to test Equation (8). The results are plotted in Figure 7, where the variables have been collected into two

Table 1. Dimensions of Fan Spray Nozzles

Nozzle designation	Orifice dimensions, cm.	Orifice projected area, sq. cm.	Water flow number, FN	Discharge coefficient, C_Q	Nozzle parameter, sq. cm. $k_0 \times 10^4$
Y	0.0305 × 0.056	0.00171	0.446	0.89	10.0
$W(i)$	0.0362 × 0.0805	0.00291	0.805	0.97	16.5
$W(ii)$	0.0370 × 0.078	0.00289	0.775	0.91	16.5
S	0.050 × 0.112	0.00560	1.55	0.95	31.5

* The complete series of photographs as well as detailed drop size distributions are to be found in reference 30.

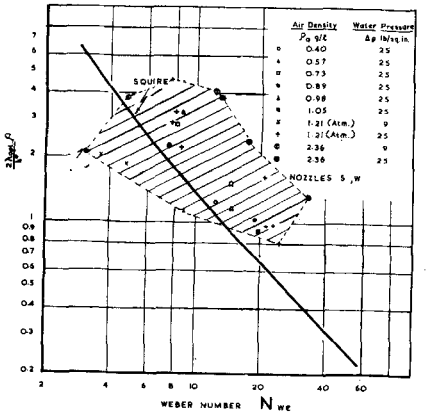

Fig. 7. Comparison of measured and calculated wave lengths.

parameters N_{we} and $\frac{\lambda_{opt}\rho}{h'}\left(=\frac{2\lambda_{opt}\rho}{h^*}\right)$. The film thickness h^* is that corresponding to the region of disintegration where λ_{opt} was measured. The curve according to Equation (7) is also included in the figure and shows reasonable agreement with theory. The experimental scatter is caused mainly from considerable irregularity in the contour of a wave front (Figures 6 and 15).

When the instability criteria $N_{we} > 1$, or > 0, are compared with experiment,* it is found that the sheets are somewhat more stable than expected and that ambient air density is a further variable, not predicted by theory. This comparison is shown in Figure 8. Instability of the sheet is characterized by the inception of waves on sheets as observed with the aid of stroboscopic light. Breakup length, measured with a cathetometer, was used to calculate sheet thickness by means of Equation (13). It will be seen from Figure 8 that near atmospheric density the criterion for instability of such sheets is $N_{we} > 1.6$ to 3. With diminishing ambient air density, the increase in N_{we} is initially gradual but becomes sharp at low density. The scatter of the experimental points also suggests that sheet thickness may be a further variable; the critical N_{we} for the thicker sheets of the larger nozzle S is consistently higher.

Values of the measured surface-volume mean diameters of the sprays are represented in Figure 9. They are found to be segregated into two groups, depending on the mode of breakup of the sheet. Equation (23) predicts that for sheets whose breakup is controlled by aerodynamic instability the mean drop diameter should be proportional to $(1/\rho_a)^{1/6}$; that is as long as the sheet is wavy, a reduction of air density causes a gradual increase in drop size

* The value of N_{we} is based on the breakup thickness h^*. The discrepancy from theory would be greater if the average thickness of the sheet had been taken.

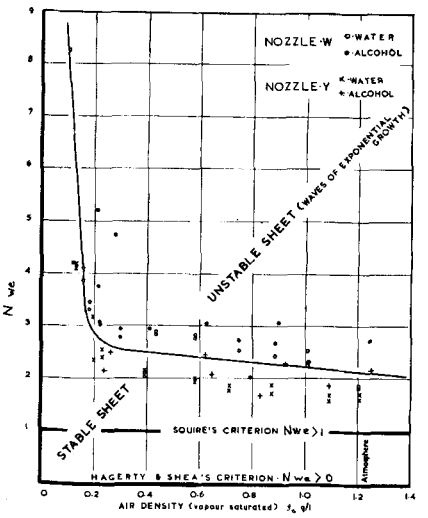

Fig. 8. Instability criterion of liquid sheets.

since the waves become less destructive. Although the amplitude growth rate decreases [$\beta_{max} \propto \rho_a$ Equation (11)] with consequent increase in breakup length, the above analysis shows that the increase in wave length [$\lambda_{opt} \propto 1/\rho_a$ Equation (10)] compensates for the reduction of sheet thickness to the extent that drop diameter increases in size according to $(1/\rho_a)^{1/6}$. The drop size data for the wavy sheets plotted in Figure 9 show a variation of the right order, but they are insufficient to test this relationship more conclusively.

It is of interest to note that the effect of air density on the drop size of other types of sprays is not dissimilar in order of magnitude, even though different breakup mechanisms are involved. The experiments of Giffen and Lamb (*24*) with injection nozzles at high air densities show that the surface-volume mean diameter varies as $(1/\rho_a)^{1/9}$, while the drop of maximum diameter varies as $(1/\rho_a)^{1/5}$. The results for twin fluid atomizers also follow the same pattern; namely Garner and Henny's (*25*) data for fuels sprayed at subatmospheric densities indicate a variation of the order of $\gamma^{0.4}(\rho_L/\rho_a)^{0.8}$. Similarly Tanasawa (*26*) has recently observed that the drop size from twin fluid atomizers varies inversely as a fractional power of the air density.

It is shown in Figure 9 that at a critical air density, where waviness has been subdued, there is an abrupt discontinuity and the drop size increases by as much as 20 to 25%. A further reduction of air density results in a small decrease in drop size, corresponding to a slightly diminished breakup thickness.

The sheet in vacuum is, at breakup, thinner than the wavy sheet in atmosphere. However it results in a coarser spray because the drops are in fact derived from thick ligaments formed

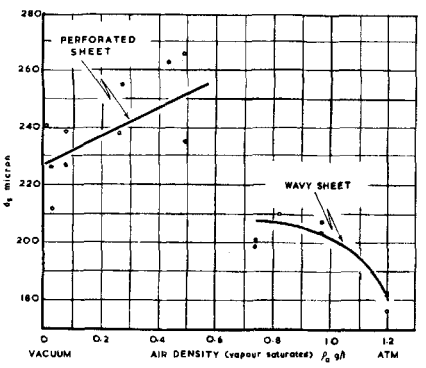

Fig. 9. Drop size at subatmospheric air density [Δp = 25 lb./sq. in. — nozzle W(*i*)].

by accumulation of the liquid originally contained in the voids of perforations of relatively large diameter.

In a further series of drop size experiments the chamber was kept at a vacuum of 28.75 in. Hg (ρ_a = 0.050 g./liter), and the differential liquid pressure was increased from 12.5 to 200 lb./sq.in. Figures 10 and 11 show values of the measured surface-volume mean diameters and of the size dispersion factors respectively. It will be seen that at all liquid pressures the spray is coarser and less uniform in vacuum.

Comparison with previous drop size results at atmospheric density can be made on the basis of Equation (23). This is given in Table 2 which summarizes available information on the drop size of fan sprays.

The magnitude of the constant C is obtained by regression of the results plotted in Figure 10 and the original data in references 2 and 27 according to the equation

$$d_s = C\left[\frac{(k_o\gamma)}{C_q^2\,\Delta p}\right]^{1/3} \qquad (25)$$

where d_s is in [μ], k_o in [sq.cm], γ in [dyne/cm.]), and Δp in [lb./sq.in.].

It is also of interest to note that other investigators (*28, 31* to *34*) studying conical spray sheets produced from swirl spray nozzles in quiescent atmosphere found empirical values for the pressure exponent lying between 0.25 to 0.35 which are not far removed from the theoretical value of 1/3, particularly if one bears in mind the experimental errors in drop size determination.

MECHANISM OF DISINTEGRATION OF THE AERODYNAMICALLY STABLE SHEET AT SUBATMOSPHERIC DENSITY

In an atmosphere the disintegration of a spray sheet is usually controlled by its aerodynamic instability. When at a sufficiently diminished air density aerodynamic stability is attained, the sheet is disrupted by perforations (Figure 6 and 15).

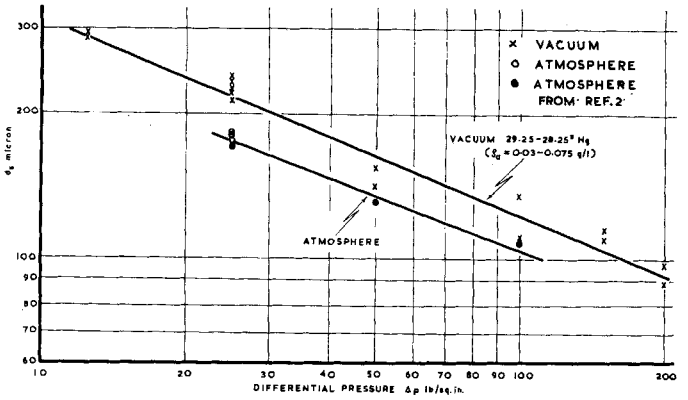

Fig. 10. Drop size at various differential pressures in vacuum and in the atmosphere [nozzle W(*i*)].

As shown above this different fundamental mode of breakup, which is not necessarily associated with low air density, has a critical effect on the drop size. The formation and behavior of perforations is therefore examined below.

Properties of Perforations

Rate of growth of a Perforation. A free boundary of a liquid sheet is subject to unbalanced surface tension forces and contracts spontaneously. Consider a small puncture in an infinitely extended sheet of uniform thickness h (Figure 12). If the puncture diameter is greater than the thickness of the sheet, there is a loss in surface area and the perforation will continue to grow. Consequently the liquid originally contained in the area of the perforation is gathered at the rim. In a perforation of radius r_p the rim is pulled outward by surface tension force $4\pi r_p\gamma$, while the opposing momentum of the liquid accumulated at the rim is

$$\rho_L \pi r_p^2 he$$

Equating force with rate of change of momentum one gets

$$4\pi r_p\gamma = \frac{\partial}{\partial t}\left[\rho_L \pi r_p^2 he\right] \qquad (26)$$

Differentiating and calling $\frac{4\gamma}{h\rho_L} = G$ one finds

$$G r_p = r_p^2 \frac{\partial e}{\partial t} + 2 r_p e \frac{\partial r_p}{\partial t} \qquad (27)$$

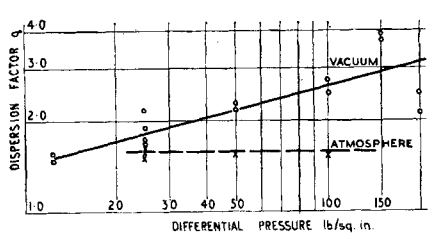

Fig. 11. Size dispersion at various differential pressures in vacuum and in the atmosphere [nozzle W(*i*)].

since

$$\frac{\partial r_p}{\partial t} = e, \text{ and } \frac{\partial e}{\partial t} = e\frac{\partial e}{\partial r_p}$$

and therefore

$$G = e\, r_p \frac{\partial e}{\partial r_p} + 2e^2 \qquad (28)$$

which, on integration, gives

$$2e^2 - G = \left[\frac{J}{r_p}\right]^4 \qquad (29)$$

where J is a constant of integration.

At the origin of a perforation $r_p = r_{po}$, where the value of r_{po} can be equal to half the sheet thickness at that point and $e = e_1$. Substituting in Equation (29) one obtains

$$J^4 = r_{po}^4\,[2e_1^2 - G]$$

so that from Equation (29)

$$2e^2 = G + \left[\frac{r_{po}}{r_p}\right]^4 (2e_1^2 - G) \qquad (30)$$

Now the average sheet thickness at which perforations originate is of the order of 3 to 5μ (Table 3). Thus when the radius of the perforation has grown to the order of 1,000μ (0.1 cm.), $r_{po} << r_p$ and $\left[\frac{r_{po}}{r_p}\right]^4$ can be neglected.

If e_1 is assumed to be of the same order as e or smaller, Equation (30) may be rewritten as

$$e = \sqrt{\frac{G}{2}} = \sqrt{\frac{2\gamma}{h\rho_L}} \qquad (31)$$

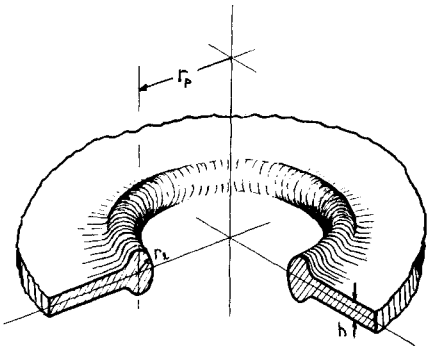

Fig. 12. Perforation in an infinitely extended liquid sheet of uniform thickness.

The growth rate of a perforation is thus independent of its radius r_p.

In applying Equation (31) to the fan spray sheet whose thickness is not uniform but varies according to $h = k_o/r$, the mean sheet thickness at the center of the perforation will be used. Equation (31) thus becomes

$$e = \sqrt{\frac{2\gamma r_d}{\rho_L k_o}} \qquad (32)$$

This equation is experimentally verified below.

It will also be realized that the rim of a perforation traveling with the fan spray sheet has an additional velocity component originating from the diverging radial streamlines.

Its effect is illustrated in Figure 13. It is seen that the initially circular hole, instead of expanding to the one represented by broken lines, is distorted to an elliptical profile which is slightly curved towards the direction of flow and flattened out in the opposite direction.

Comparison with Experiment. The validity of Equation (32) has been confirmed by measuring growth rates of perforations, from double exposure photographs of water sheets in vacuum, with two sizes of nozzle at two differential pressures.

A perforation growth rate e in a sheet of velocity U_o was conveniently obtained from the movement of points similar to B and C, lying on the intersections of the rim with the radial line 00′ (Figure 13). At such points the resultant velocity is on the same axis

Table 2. Drop Size of Fan Sprays

Author	Ambient conditions	Nozzle parameter, $k_o \times 10^4$ sq. cm.	Injection pressure, Δp lb./sq. in.	C.
Dorman (27)	Atmosphere	21.1 to 1,011	50 to 105	942
Straus (2)	Atmosphere	21.1 to 45.5	25 to 100	920
Present authors	28.75 in Hg vacuum	16.5	12.5 to 200	1,172.5

TABLE 3. CHARACTERISTICS OF PERFORATED SHEETS OF WATER IN VACUUM

Nozzle	Δp lb./sq. in.	Measured radii of holes r_p, cm.	Observed position of holes r_d, cm.	Origins of holes: Calculated r_i, cm.	Origins of holes: Measured (average) r_i, cm.	Average sheet thickness at origin of perforation μ	Distances moved from origin $r_d - r_i$, cm.	Velocity of growth of perforation e, cm./sec.
W	25	0.13 to 0.37	4.42 to 6.29	3.27 to 5.56	4.47	3.7	0.34 to 1.15	580 to 760
	49	0.11 to 0.66	4.19 to 7.38	2.02 to 7.04	4.73	3.5	0.34 to 2.50	600 to 830
S	25	0.11 to 0.66	6.43 to 8.34	4.58 to 6.80	6.07	5.2	0.36 to 2.00	450 to 640
	49	0.17 to 0.48	5.04 to 8.15	3.73 to 7.11	5.75	5.5	0.79 to 2.18	440 to 660

		Sheet velocity U_o, cm./sec.	Breakup length of sheets r^*, cm.	Average breakup length r^*, cm.	Widths of sheets at breakup s^*, cm.	Average breakup width s^*, cm.	Average breakup thickness h^*, μ	Average breakup thickness in atmosphere h^*, μ
W	25	1,800	6.2 to 9.4	7.7	1.8 to 3.6	3.0	2.1	3.1
	49	2,520	8.2 to 12.7	9.4	4.2 to 6.4	5.6	1.8	3.8
S	25	1.770	9.0 to 13.2	11.9	4.5 to 6.0	5.2	2.6	6.1
	49	2,480	8.7 to 11.6	10.3	7.0 to 8.0	7.4	3.1	8.3

as the individual components e and U_o, and

$$e = \frac{CC' - BB'}{2\,\Delta t} \qquad (33)$$

Experimental values of e against the mean radial distance are plotted in Figure 14 and show reasonable agreement with the curves calculated in accordance with Equation (32). The experimental scatter arises from the irregularity in the contour of a perforation and its lack of sharpness in the photographs.

The photographs have also been used to determine the velocity of the drops in the immediate zone of disintegration of the spray sheet. Measurements were confined to drops above 100-μ diam. for which successive positions could be easily identified. It was found that the velocity of the majority of drops is essentially identical to that of the sheet, only a small percentage moving either faster or slower. The latter drops originate from ligaments formed by the impact of rims of unequal mass which are produced from adjacent perforations with dissimilar histories. An additional velocity component is therefore imposed on the ligament.

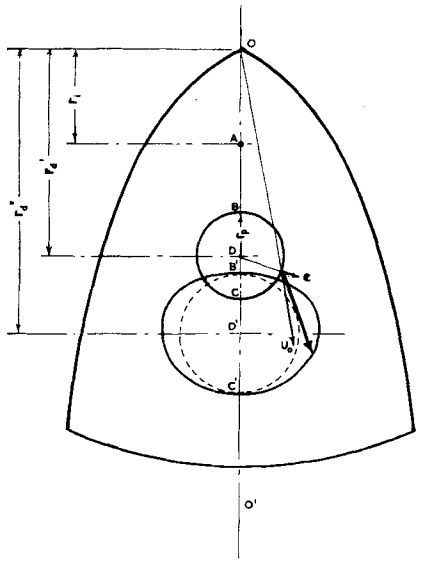

Fig. 13. Consecutive positions of one perforation.

Origins of Perforations. Equation (32) will now be extended to give an expression for the location of the origin of an observed hole.

Consider a perforation of negligible size, just appearing at a point A situated at a radial distance r_i from the orifice (Figure 13). After t sec. the perforation center has traveled to a distance r_d. The perforation radius r_p measured along the axis CO' increases at the rate

$$e = \frac{\partial r_p}{\partial t} = \sqrt{\frac{2\gamma r_d}{\rho_L k_o}} \qquad (34)$$

Since the velocity U_o is constant along the sheet (9)

$$r_d = r_i + U_o t \qquad (35)$$

Substituting for r_d one finds

$$r_p = \sqrt{\frac{2\gamma}{\rho_L k_o}} \int_o^t \sqrt{r_i + U_o t}\,\partial t \qquad (36)$$

or

$$r_i^{3/2} = r_d^{3/2} - \frac{3}{2} r_p U_o \sqrt{\frac{\rho_L k_o}{2\gamma}} \qquad (37)$$

Equation (37) has been used to obtain information on the location of the origins of perforations. Since no two photographs taken under nominally similar conditions give the same number and distribution of perforations, it is possible to deal only in terms of ranges and averages. Table 3 gives the order of magnitude involved, based on measurements from numerous photographs of water sprays in a vacuum of 28¾ in. Hg.

For the typical sprays considered the average perforation originates in the central region of the sheet, and its radius is usually less than 1 cm. Its lifetime is of the order of 1 msec., and it travels only a short distance of about 0.5 to 2.5 cm. before coalescing with other perforations.

Most of the perforations recorded in Table 3 were observed at the lower end of the sheet. Examination of spray sheets in vacuum over a wider range of injection pressure reaching 900 lb./sq.in. has shown that consistent perforations in the upper part of the sheet occur only at the highest pressures. However under these conditions a different mechanism of hole formation is probably involved.

Causation of Perforations

In a previous investigation (*1*) it was shown that nonwettable particles in a heterogeneous liquid, such as an oil/water emulsion or an aqueous wax particle suspension, are responsible

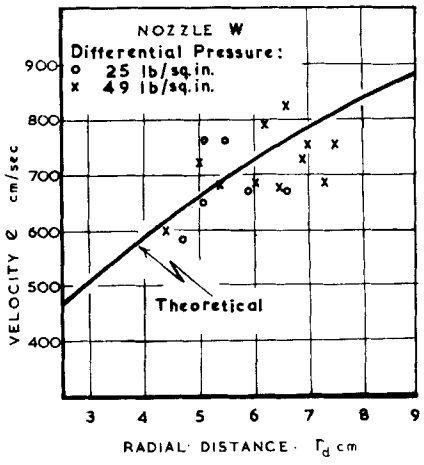

Fig. 14. Comparison of measured and calculated rates of growth of perforations.

for the large number of perforations formed on the spray sheet, and this is not unexpected. There is however no apparent reason for the sheet of a homogeneous pure liquid in laminar flow under vacuum conditions to be punctured.

Effects of Dissolved and Entrained Gases. It was thought that the perforations might be caused by release of microbubbles from dissolved air, as a consequence of the pressure drop at the orifice. To test this hypothesis distilled water was deaerated to an air content low enough to prevent bubbling out. Spray sheets of aerated and deaerated water were examined in a vacuum of 28½ in. Hg and in the atmosphere with two nozzles W and S (Table 1) and liquid pressures up to 50 lb./sq. in. It was found that air content of the liquid made no difference in the appearance or size of the spray sheet and had no effect on the recurrence of perforations. This result was confirmed by a second series of similar experiments in which care was taken to eliminate air or vapor trapped in the pipe system by connecting the feed vessel to the nozzle with a single piece of tubing.

It is therefore concluded that perforations originate neither from release of a dissolved gas nor from cavitation, since this phenomenon does not readily occur with water of low air content.

Ripple Effects. When the fan spray sheet in vacuum is photographed with specular illumination (7), its surface is found to be disturbed by numerous point and longitudinal marks surrounded by ripples. High speed cine photographs show that although the disturbance surrounded by ripples need not necessarily develop into a perforation, it is a prerequisite for the latter to be formed.

Similar ripples, observed on the unruffled perforated sheets of mercury flowing in atmosphere, have been reported previously (*1, 10*). Data then available suggested that their formation is associated with vibration in the nozzle orifice at high Reynolds numbers (*8*). Further work has shown however that ripples appear also at low Reynolds numbers as well as with liquids of widely ranging properties and at different ambient conditions. These facts can be explained by an alternative explanation postulating that ripples and the resulting perforations are caused by particles impinging on the sheet surface. The latter hypothesis is also supported by experiments showing that a drop made to impinge on the sheet produces a perforation surrounded by ripples or only ripples which ultimately may develop into a puncture.

The characteristic perforations on the sheet in vacuum remain unaltered when various baffle configurations are arranged inside the chamber. Moreover perforations are not eliminated when the sheet is protected against drops ricocheting from the walls of the chamber by the use of two glass plates situated close and parallel to the plane of the sheet. It follows that if ripples and perforations are caused by impinging particles, the drops must be projected from the orifice or the sheet itself and the phenomenon is independent of vessel geometry.

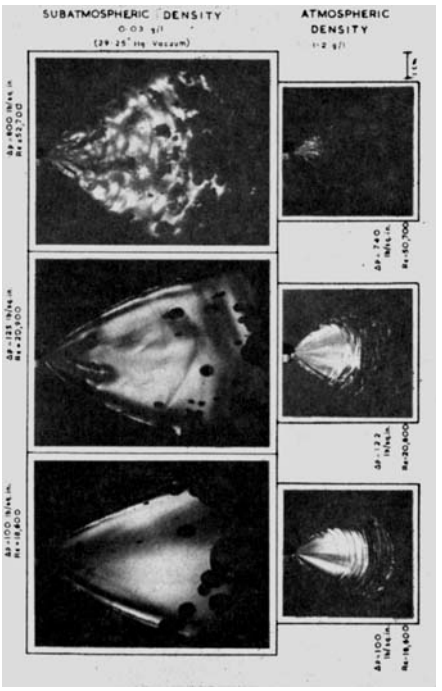

Fig. 15. The effect of differential injection pressure on the turbulence in liquid sheets.

It is difficult to explain the mechanism by which impinging drops follow a trajectory close to the sheet and leading back to the sheet surface. There is some evidence that the drops originate at the orifice where a high rate of shear exists because at high differential pressures streams of drops have been observed to originate from the orifice and to produce a row of holes oriented along a streamline (*30*). However as yet there is no direct proof that this phenomenon occurs at low injection pressures.

TURBULENCE INSTABILITY OF A LIQUID SHEET

In a thick liquid sheet flowing in quiescent atmosphere irregular ridges and cavities are superimposed on the highly unstable aerodynamic waves, giving it a highly turbulent appearance. To investigate the character of this turbulence high velocity water sheets have been examined under conditions of aerodynamic stability, that is in ambient vacuum.

Figure 15 shows the development of turbulence with increasing pressure on sheets in vacuum, produced by the intermediate size nozzle *W*. Photographs of corresponding sheets flowing in atmosphere have been included for comparison. At low liquid pressure the sheet in vacuum is perfectly flat, to the extent that it reveals interference fringes (*9*). At medium pressure the sheet is semiturbulent, but traces of the fringes are still apparent. At high pressure the sheet is turbulent, the entire surface being disturbed by highly irregular waves. These waves are quite distinct from the exponentially growing aerodynamic waves which are pronounced only in the lower portion of a sheet.

Surprisingly the maximum breakup length of the sheet in vacuum remains almost constant, up to high pressure of 800 lb./sq.in. Under ambient vacuum conditions a sheet disintegrates by the coalescence of rapidly growing perforations. At a high sheet velocity the time available for their growth is less. Since the breakup length is found not to vary, it follows that the frequency of perforations must increase with sheet velocity, a larger number of smaller holes keeping the breakup length constant.

Table 4 gives the Reynolds numbers for laminar, semiturbulent, and turbulent flow for the sheets produced by the nozzles listed in Table 1.

TABLE 4. TURBULENCE CRITERION OF FLAT SHEETS

Nozzle	Injection pressures, lb./sq.in. Laminar	Semi-turbulent	Turbulent	Reynolds numbers Laminar	Semi-turbulent	Turbulent
Y	0 to 250	300 to 450	>600	0 to 23,200	25,400 to 31,100	>35,900
W	0 to 110	115 to 200	>400	0 to 19,600	21,400 to 26,400	>37,300
S	0 to 12.5	15 to 25	>50	0 to 9,200	10,000 to 13,000	>18,400

Nozzle	Sheet thickness at breakup in vacuum h^*, μ	Orifice dimensions, cm.	Hydraulic mean diameter, cm.
Y	1.4	0.056 × 0.0305	0.0395
W	1.0	0.078 × 0.037	0.0502
S	3.1	0.112 × 0.050	0.0701

The critical Reynolds number at which turbulence appears in a flat sheet lies in the range of 18,000 to 37,000. These figures agree with the range $N_{Re} = 20{,}000$ to 40,000 quoted by Dombrowski and Fraser (*1*), although a different turbulence criterion was applied; namely turbulence was identified with the occurrence of perforations.

Previous investigations of jets in vacuum (*17, 18*), have established that critical Reynolds numbers of jets are similar to those for pipe flow, namely $N_{Re} = 2{,}000$ to 3,000. In a more recent study of water jets in atmosphere Panasenkov (*19*) and Borisenko (*23*) observed a maximum of the breakup length at $N_{Re} = 4{,}000$ to 4,500 and claimed that this was the criterion for jet turbulence. Their conclusion is doubtful since the maximum can be explained without postulating turbulence.

Comparison of the turbulence criteria shows that liquid sheets are considerably more stable than plain jets issuing from orifices of the same area.

The relative importance of aerodynamics and turbulence effects in the disruption of high speed jets is controversial (*17, 18, 20, 21, 22*). The results of this investigation suggest that, in the case of liquid sheets, turbulence plays only a minor role and does not appear to assist the atomization process to any significant extent, either in vacuum or in atmosphere. In Figure 10 the transition from laminar to semi-turbulent flow occurring at 110 lb./sq. in. pressure (Table 4) is not reflected in any discontinuity in the variation of the drop size in vacuum. A wider range of Reynolds numbers has been covered in previous investigations of fan sprays in the atmosphere, and no special effect of turbulence on drop size can be noticed. However these conditions do not cover the fully turbulent region.

NOTATION

A = projected area of orifice
C = constant [Equation (25)]
C_q = discharge coefficient
C_v = velocity coefficient
d = drop diameter
d_s = surface-volume mean diameter
$d_{5\%}$ = 5% oversize diameter
$d_{95\%}$ = 95% oversize diameter
E = dimensionless wave amplitude ratio, $\ln \frac{y^*}{y_o}$
e = expansion velocity of rim of perforation at radius r_p
FN = flow number
f = wave frequency
g_c = gravitational conversion factor
$G = \frac{4\gamma}{h\rho_L}$
h = thickness of fan spray sheet at radial distance r
h' = half sheet thickness $h/2$
h^* = breakup thickness of fan spray sheet
J = constant [Equation (29)]
k_o = parameter of fan spray nozzle
k = wave number, $2\pi/\lambda$
m = hydraulic mean diameter of orifice
N_{Re} = Reynolds number, $m U_o \rho_L/\eta$
N_{We} = Weber number, $\frac{\rho_L U^2 h^*}{2\gamma}$
Δp = differential injection pressure
Q = volumetric discharge rate
q = size dispersion
r = radial distance measured from orifice
r^* = maximum breakup length of a fan spray sheet
r_d = radial distance from orifice to center of perforation
r_l = radius of ligament
r_i = radial distance from orifice to origin of perforation
r_p = radius of perforation
r_{po} = radius of perforation at origin
t = time
Δt = time interval
U_o = sheet velocity
V = wave velocity
w = circular frequency $2\pi f$
y = amplitude of wave at time t
y_o = initial wave amplitude at orifice
y^* = wave amplitude at breakup

Greek Letters

β = exponential growth rate of wave amplitude
γ = surface tension
η = absolute liquid viscosity
λ = wave length
λ_{min} = wave length for minimum instability
λ_{opt} = wave length for maximum growth rate
ρ = air/liquid density ratio ρ_a/ρ_L
ρ_a = air density
ρ_L = liquid density

LITERATURE CITED

1. Dombrowski, Norman, and R. P. Fraser, *Phil. Trans. Roy. Soc. London*, **247A**, 101 (1954).
2. Fraser, R. P., and Paul Eisenklam, *Trans. Inst. Chem. Engrs. (London)*, **34**, 294 (1956); Straus, R., Ph.D. thesis, London Univ., London, England (1949).
3. Bowen, I. G., and G. P. Davies, *Shell Tech. Note ICT/28* (1951).
4. Nukiyama, A. S., and Y. Tanasawa, *Trans. Soc. Mech. Eng. Japan*, **4**, 86 (1938).
5. Tate, R. W., and W. R. Marshall, *Chem. Eng. Progr.*, **49**, 169 (1953).
6. Heywood, H., *Proc. Inst. Mech. Engrs. (London)*, **125**, 383 (1933).
7. Fraser, R. P., and Norman Dombrowski, "Proceedings Third International Congress High Speed Photography," p. 376, Butterworths, London, England (1956).
8. ———, and Paul Eisenklam, *Nature*, **173**, 495 (1954).
9. Dombrowski, Norman, David Hasson, and D. E. Ward, *Chem. Eng. Sci.*, **12**, 35 (1960).
10. Dombrowski, Norman, and Paul Eisenklam, *Agr. Research Council Rep. ARC/198/52*, No. 21064 (1952).
11. Rayleigh, Lord, Proc. *Lond. Math. Soc.*, **10**, 4 (1878/9).
12. Weber, C., *Z. Angew. Math. & Mech.*, **22**, 509 (1931).
13. Squire, H. B., *Brit. J. Appl. Phys.*, **4**, 167 (1953).
14. Hagerty, W. W., and J. F. Shea, *J. Appl. Mech.*, **22**, 509 (1955).
17. De-Juhasz, K. J., O. F. Zahn, and P. H. Schweitzer, *Bull. Penns. State College Eng. Expt. Sta.*, No. 40 (1932).
18. Lee, D. W., and R. C. Spencer, *Natl. Advisory Comm. Aeronaut. Ann. Rept. No. 454* (1933).
19. Panasenkov, N. S., *J. Tech. Phys. (U.S.S.R.)*, **21**, 160 (1951).
20. Castleman, R. A., *J. Res. Nat. Bur. Standards*, **6**, 369 (1931).
21. Hinze, J. O., *Appl. Sci. Research*, **A1**, 273 (1949).
22. Merrington, A. C., and E. G. Richardson, *Proc. Phys. Soc. (London)*, **59**, 1 (1947).
23. Borisenko, A. I., *J. Tech. Phys. (U.S.S.R.)*, **23**, 195 (1953).
24. Giffen, E., and T. A. J. Lamb, *Motor Ind. Res. Assocn. Rep. No. 1953/5* (1953).
25. Garner, F. H., and V. E. Henny, *Fuel*, **32**, 151 (1953).
26. Tanasawa, Y., Private communication from Tohuku University, Japan (1958).
27. Dorman, R. G., *Brit. J. Appl. Phys.*, **3**, 189 (1952).
28. Turner, G. M., and R. W. Moulton, *Chem. Eng. Progr.*, **49**, 185 (1953).
29. Keller, J. B., and I. Kolodner, *J. Appl. Phys.*, **25**, 918 (1954).
30. Hasson, David., Ph.D. thesis, London Univ., London, England (1956).
31. Joyce, J. R., *J. Inst. Fuel*, **22**, 150 (1949).
32. Longwell, J. P., D.Sc. thesis, *Mass. Inst. Technol.*, Cambridge, Massachusetts (1943).
33. Needham, H. C., Unpublished M.O.A. report (1946).
34. Radcliffe, A., *Proc. Inst. Mech. Eng.*, **169**, 93 (1955).

Manuscript received December 29, 1960; revision received March 16, 1962; paper accepted March 19, 1962.